

Recognition and Estimation of Human Finger Pointing with an RGB Camera for Robot Directive

Eran Bamani, Eden Nissinman, Lisa Koenigsberg, Inbar Meir, Yoav Matalon and Avishai Sintov

Abstract—In communication between humans, gestures are often preferred or complementary to verbal expression since the former offers better spatial referral. Finger pointing gesture conveys vital information regarding some point of interest in the environment. In human-robot interaction, a user can easily direct a robot to a target location, for example, in search and rescue or factory assistance. State-of-the-art approaches for visual pointing estimation often rely on depth cameras, are limited to indoor environments and provide discrete predictions between limited targets. In this paper, we explore the learning of models for robots to understand pointing directives in various indoor and outdoor environments solely based on a single RGB camera. A novel framework is proposed which includes a designated model termed *PointingNet*. *PointingNet* recognizes the occurrence of pointing followed by approximating the position and direction of the index finger. The model relies on a novel segmentation model for masking any lifted arm. While state-of-the-art human pose estimation models provide poor pointing angle estimation accuracy of 28° , *PointingNet* exhibits mean accuracy of less than 2° . With the pointing information, the target is computed followed by planning and motion of the robot. The framework is evaluated on two robotic systems yielding accurate target reaching.

I. INTRODUCTION

FINGER Finger pointing is a universal gesture where a human extends the arm and index finger in direction of a desired target [1]. As such, it is a prominent form of communication between humans in various cultures in order to direct attention to some region of interest in the environment [2]. Tomasello [3] argued that gestures, and pointing in particular, preceded vocal communications as gestures provide better spatial referral than speech. Pointing naturally and rapidly directs human attention to external targets while speech does not. Infants, for instance, use pointing before they learn to pronounce words [4]. Furthermore, in multi-cultural interaction, pointing is the preferred form of communication to cope with the language barrier [5]. Consequently, pointing is an indispensable tool for conveying important information. Pointing recognition in Human-Robot Interaction (HRI), therefore, is a necessary form of communication for natural and easy directives to robots.

HRI is a wide field of study that explores means of mutual interaction between humans and robots. An interaction between a human and a robot might occur in the form of information exchange, collaboration or guidance. In general, gesture recognition is a popular non-verbal approach for HRI



Fig. 1. A user directs a quadruped robot to a target position by pointing. The robot observes the user through an RGB camera. *PointingNet* identifies a pointing gesture and estimates its position and direction. Once the target has been calculated, the robot plans motion and moves to the target.

and has historically been approached by conventional classification techniques utilizing handcrafted features [6]–[8]. Nevertheless, these methods have been found to be weak against the complexity of human motions. Consequently, significant effort has been put in modeling and understanding intents of human users through natural gestures [9]. By using natural human gestures, and mainly pointing as done between humans, directive instructions to a robot can easily be commanded while reducing the cognitive burden imposed on the user [10]. The cognitive load on users can be reduced as they do not have to spend much mental effort learning and remembering complex commands or navigating through menus of digital interfaces. For instance, first responders can instantly direct a robot to assist while performing life saving tasks. Similarly, medical personnel can direct a robot to fetch tools or supplies.

In order for a robot to understand the pointing gesture of a human, it must first recognize the occurrence of pointing and then estimate direction. Various approaches have been proposed for the estimation of pointing direction while few addressed the recognition problem. Direction estimation methods can be divided into two categories based on the sensing modality: wearable devices and visual perception. Work with wearable devices for pointing estimation have used Inertial Measurement Units (IMU) [11] and Electro-Myography (EMG) [12] to sense motion and pose of the arm. However, these devices often require constant carrying of

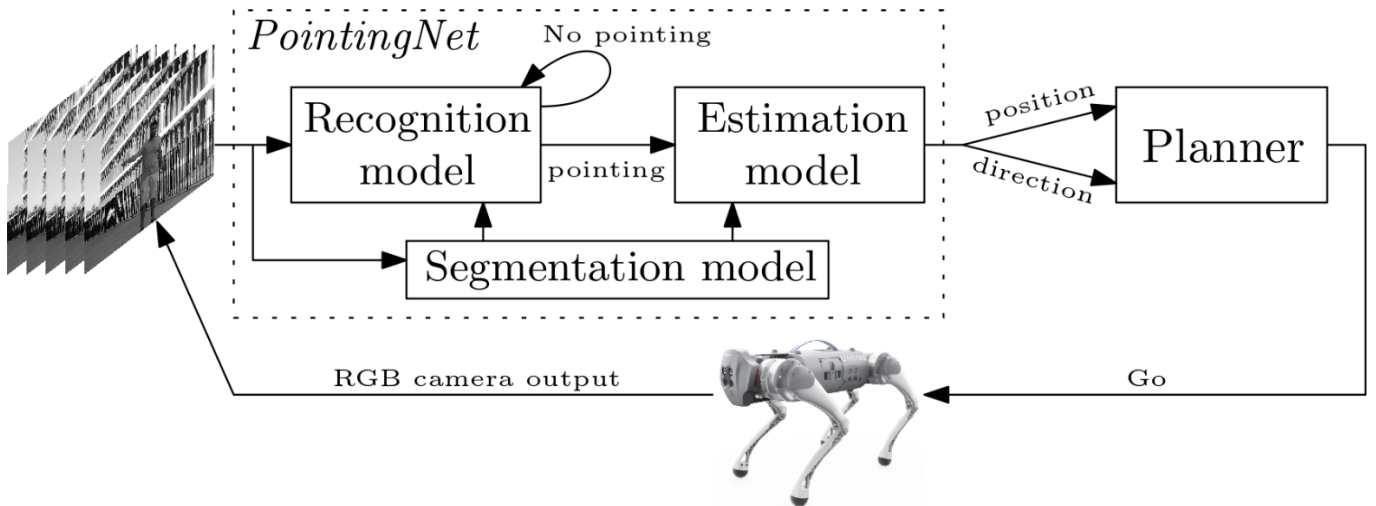


Fig. 2. Illustration of the proposed framework for a robot reach to a pointed target. Pointing recognition acts as a trigger. That is, once pointing of the user has been identified, the pointing position and direction are estimated and used by the planner for planning the motion of the robot in the instructed direction.

the sensors along with micro-controllers on the user’s body, which may be cumbersome. More importantly, they prevent spontaneous pointing towards a robot and ability for occasional users to direct it.

As opposed to wearable sensing, visual perception allows spontaneous observation of any frequent user with one or more cameras. Much work has been done on pointing detection using multiple RGB cameras or a depth (stereo) camera [13]–[15]. Nickel and Stiefelhagen [16], for instance, used a depth camera along with a prior probabilistic body model in order to observe the forearm and head, and identify direction of pointing gestures. While depth data enables easier access to pointing gestures, depth cameras are limited to short-range in indoor environments and work poorly outdoors. In addition, they require an additional hardware setup and limit the generality of the method [17]. However, only few addressed the pointing problem using a single RGB camera [18]. The work in [19] used a simple monocular camera along with a classifier to predict the target on an indoor floor from a set of discrete points in the proximal surroundings of the user. Features from both the arm and head were extracted and initiation of estimation was triggered using voice commands. In [17], detection of whether the hand is pointing on objects was performed. The detection was conducted with a camera set above the table in a constructed environment. A Convex-Hull (CH) of the hand assisted in verifying that exactly one finger is stretched out. However, the method was limited to detection from a specific camera angle and other directions were not demonstrated. Also, the work is restricted to a table top scenario with a small viewing angle. These few methods that utilize only a single RGB camera are demonstrated in a limited setting while considering rough estimation of pointing direction toward large objects.

Many advances in HRI rely on human pose estimation models often termed *Skeleton* models. These models use either depth or RGB cameras to find a set of key-points that can represent the pose of the human body. Recent work used the

OpenPose library [20] to extract a 2D skeleton model of the user from a single RGB camera [18]. Spatial pose of the user’s arm was extracted from the 2D image by calibration of fixed distances of a specific human user. This makes the method designated for only a single user while the pointing accuracy is not clear. Then, the pointing direction is extracted analytically from the detected arm joints and was used to direct a drone to one of several building windows. Pointing direction estimation using prominent skeleton models (e.g., MediaPipe [21], VNect [22], OpenPose [23]) provide real-time 3D pose estimation with a simple RGB camera. Results to be presented in this work show that these models provide poor results that cannot be used for accurate prediction of pointing direction. In addition, the key-points of the skeleton are provided with respect to some root and not relative to the camera. Hence, arm location relative to the robot equipped with a camera cannot be acquired.

In order for the robot to infer the target that the user is pointing to, the robot must accurately estimate the position of the finger and its direction with respect to the robot’s coordinate frame. The accuracy is even more important in an environment with poor diversity [24]. For example, when commanded through pointing to go to a specific window out of many in a building, a search and rescue drone must accurately identify the correct one. Slight variations in estimation may result in failure. Some approaches measure pointing by the direction of the forearm [12], the index finger [25] or the vector formed by the root of the nose and index finger [26]. However, no thorough analysis was performed to determine the pointing measurement that best reflects the intent of the user. Most approaches are based on forearm direction estimation [27], [28]. Yet, the forearm and index finger are not always co-linear while the index finger is considered more accurate in pointing. Work that attempted to estimate the direction of the index finger focused on a limited discrete setting and solved a classification problem to distinguish between several objects on an indoor table top [25], [29]. In conclusion and

to the best of the authors knowledge, no work has addressed a continuous pointing estimation problem based on observing the index finger by an RGB camera while able to work indoor and outdoor, and to recognize the occurrence of pointing.

In this paper, we investigate the ability to learn robust models for pointing recognition and estimation in diverse environments. The aim is for a mobile robot to recognize pointing, estimate target location and move to it (Figure 1). First, a thorough experimental analysis is provided in order to determine the accuracy of the three pointing measurement approaches. Then, a full framework for accurate pointing recognition and estimation is proposed solely based on RGB images. The framework is illustrated in Figure 2. A novel model termed *PointingNet* is proposed in which two main components are the pointing recognition and estimation models. Both models are based on a unique segmentation model aimed to mask any lifted arm in the scene. Then, the recognition model classifies the segmented arm in order to determine whether pointing is exhibited. If so, a novel estimation model is triggered to approximate the position and direction of the index finger with respect to the camera. The robot, in turn, computes the desired target and moves towards it. To summarize, the contributions of this work are as follows:

- A comparative analysis is presented for measurement approaches of pointing direction considering the intended target of the user.
- The framework includes a recognition model that identifies when the user is pointing.
- A novel pointing estimation model is proposed for estimating the position and direction of the index finger during pointing. Evaluation over a diverse test set shows highly accurate estimations.
- A unique segmentation model is used in order to focus the recognition and estimation on the pointing arm. The segmentation model outputs a mask for any visibly lifted arm in the image.
- Unlike prior work, the proposed models are based on a simple RGB camera and can provide continuous estimations in various indoor and outdoor environments based solely on observation of the user’s arm.
- The proposed framework is demonstrated and evaluated on two mobile robots.
- Trained model and labeled pointing dataset are available open-source for the benefit of the community¹.

The method proposed in this work has potential applications in additional areas such as virtual and augmented reality, interactive presentations and directive reasoning of various other gestures. In addition, the approach can be used in gaming and theme-parks to enable participants the interaction with a game environment through natural gestures. In this work, we assume that the camera is on the robot and, therefore, reference is with respect to the robot. However, an alternative application can have a designated station with a camera for the user to naturally direct or tele-operate a remote robot.

II. RELATED WORK

Existing methods for point detection can be divided into three categories based on the used sensing system: depth camera, RGB camera and wearable device. The majority of work with visual perception are based on depth cameras or multiple RGB ones from different pointing views. Early work used depth camera images to estimate the pointing targets on a table [13]. Nickel and Stiefelhagen [16] identified direction of pointing gestures through head and hands by clustering human skin color based on [34]. The body model is also used along with a Hidden Markov model to detect the occurrence of pointing. Another method detected and approximated the pointing direction from two orthogonal camera views [25]. Recently, two fish-eye cameras were installed on both sides of a display and used to capture images of a wide area in front of the display. With such setting, the system can recognize the user’s skeleton and estimate pointing direction towards the display [28]. Similar work [35] relied on contour detection along with CH of the hand while using close-up Kinect-based images of hands. Hence, it is not clear whether the method is applicable for real world scenarios.

Finger data is not easy to extract in an unconstructed environment due to its small area it occupies in the image. Hence, some work observes alternative or additional body features. The common approach is to determine pointing direction based on the forearm posture [16], [28]. The work in [27], [30] used a depth camera to identify the vector formed by the elbow and wrist extracted from a skeleton model [36]. Intersection of the vector with the floor was then computed in order to determine the desired goal location for a mobile robot. Note that in [27], detection of a pointing gesture was performed by solely observing whether the height of the arm is within some threshold relative to the shoulder. A different approach detected the positions of the head and hand with a depth camera, and considered the vector connecting them as the pointing direction [26]. In the same work, the hand closest to the camera was heuristically chosen as the pointing one. The work in [29], on the other hand, proposed a method that solely observes the hand independent of body postures. The work offered a model-free probabilistic method to identify the pointed object from a known set. However, the work relied on a depth camera in a limited setting of a single viewing angle above a tabletop.

While visual perception is the leading approach for pointing and gesture recognition, a different approach worth mentioning is the use of wearable devices. For instance, two Inertial Measurement Units (IMU) were positioned on the forearm of a user during pointing on a presentation screen [11]. Often, Electro-Myography (EMG) is used alongside an IMU. In EMG, electrical muscle signals are sensed and mapped to limb movements [37]. While an IMU can approximate motion and posture, EMG can also provide hand gesture recognition. EMG along with an IMU was used for gesture recognition and detection of forearm pointing direction [12]. Similarly, EMG and IMU were used on the user’s forearm to control a drone through obstacles [38]. However, IMU is prone to drift and requires frequent calibrations [17]. A different approach used

¹To be available upon acceptance for publication. Images will be modified in order to protect the privacy of the participants.

TABLE I
STATE-OF-THE-ART COMPARISON OF POINTING RECOGNITION METHODS

Paper	Recognition	Body posture	Skeleton	IF/FA/EF	Indoor	Outdoor	RGB/Depth/Wearable	Continuous/Discrete
Sikeridis et al. [11]	✗	✗	-	FA	-	-	Wearable	C
Haque et al. [12]	✓	✗	-	FA	-	-	Wearable	C
Nickel and Stiefelhagen [16]	✓	✓	✗	FA/EF	✓	✗	Depth	C
Jirak et al. [17]	✓	✗	✗	IF	✓	✗	RGB	D
Medeiros et al. [18]	✗	✓	✓	FA	✗	✓	RGB	D
Martin et al. [19]	✗	✓	✗	-	✓	✗	RGB	D
Hu et a. [25]	✗	✗	✗	IF	✓	✗	2×RGB	C
Azari et al. [26]	✗	✓	✗	EF	✓	✗	Depth	C
Lai et al. [27]	✓	✓	✓	FA	✓	✗	Depth	C
Kuramochi et al. [28]	✗	✗	✓	FA	✓	✗	2×RGB	C
Shukla et al. [29]	✗	✗	✗	IF	✓	✗	Depth	D
Tölgyessy et al. [30]	✗	✗	✓	FA	✓	✗	Depth	C
Pietroszek et al. [31]	✗	✗	-	FA	-	-	Wearable	C
Das [32]	✗	✗	✗	IF	✓	✗	Depth	C
Kehl and Van Gool [33]	✓	✓	✗	EF	✓	✗	8×RGB	C
Proposed method	✓	✗	✗	IF	✓	✓	RGB	C

an off-the-shelf smartwatch to point and interact with a large display [31]. As mentioned in the previous section, wearable devices require carrying hardware on the body and prevent spontaneous or occasional pointing by arbitrary users.

Table I summarizes the state-of-the-art on pointing detection and estimation. The table sorts various characteristics of prior methods which include the following. *Recognition*: whether the proposed method identifies the occurrence of pointing; *Body posture*: whether the method requires some body posture information in addition to the arm; *Skeleton*: whether the method utilizes some skeleton library for human pose estimation; *IF/FA/EF*: whether the method observes the direction of the Index Finger (IF), Forearm (FA) or Eyes-Finger (EF) vector; *Indoor/Outdoor*: was the method demonstrated in indoor and outdoor environments; *RGB/Depth/Wearable*: what is the sensing technology used for pointing data acquisition; and, *Continuous/Discrete*: does the method provide continuous pointing estimation or classifies from a discrete set of regions or objects. The table shows high dependence of vision-based methods on depth cameras and, therefore, the majority of the methods cannot be used outdoors. In addition, forearm detection is the leading approach while observing the index finger is less common, and with RGB camera in particular.

III. PRELIMINARY POINTING ANALYSIS

As discussed above, prior pointing work considered the measurement of either the forearm (FA) vector formed by the wrist and elbow points [16], [28], index finger (IF) direction [17] or the direction of the vector connecting the user eyes (root of nose) and finger (EF) [16], [26], [33]. Illustration of these measurement types is seen in Figure 3. Yet and to the best of the authors knowledge, a thorough experimental comparison between the three measurement approaches has never been conducted.

Irrelevant of the hardware and any learning method to estimate the pointing direction, we wish to examine how accurate is each of the measuring approaches. Hence, an experiment was designed and conducted in which seven participants were asked to point towards a pre-defined target. Several reflective

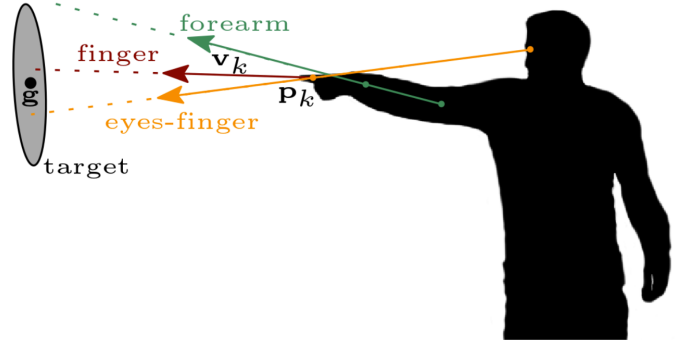


Fig. 3. Three approaches for measuring pointing direction: forearm vector formed by the wrist and elbow points, index finger vector and the vector connecting the user eyes and finger. Pointing error e_k is calculated according to the minimal distance between the target center point \mathbf{g} and the calculated direction vector \mathbf{v}_k passing through some key-point \mathbf{p}_k where $k = \{\text{FA}, \text{IF}, \text{EF}\}$.

markers were positioned on designated eyeglasses, finger (Figure 7b) and forearm (wrist and elbow) of the user as well as on the target. Using a motion capture system, the target position along with poses of user index finger, forearm and root of the nose were captured during pointing to the target. Users were instructed to point to the target in various positions with respect to the target and various body poses such as standing, sitting down and crouching. Also, the users were specifically asked to look at the target during pointing. For each measuring approach, the pointing direction $\mathbf{v}_k \in \mathbb{R}^3$ and a key-point $\mathbf{p}_k \in \mathbb{R}^3$ were calculated where $k = \{\text{FA}, \text{IF}, \text{EF}\}$. The key-point is the position of the pointing finger for IF and EF approaches, or wrist for FA approach. Then, the pointing error e_k is the minimal distance between a line in direction \mathbf{v}_k passing through \mathbf{p}_k and the target center point $\mathbf{g} \in \mathbb{R}^3$, given by

$$e_k = \frac{\|(\mathbf{g} - \mathbf{p}_k) \times \mathbf{v}_k\|}{\|\mathbf{v}_k\|}. \quad (1)$$

Note that the experiment does not consider gaze but solely the position of the root of the nose as commonly done in pointing recognition work. Measuring gaze usually requires a camera fixed on the head of the user tracking pupil directions.

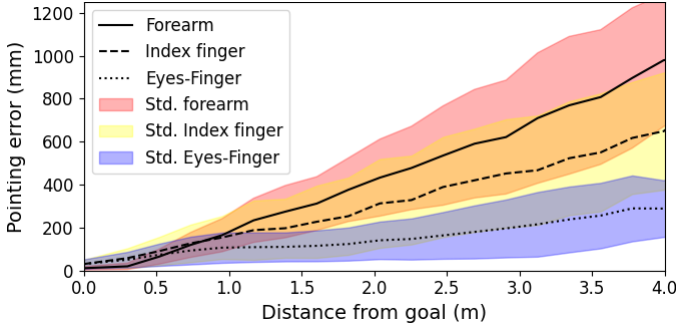


Fig. 4. Pointing accuracy with regards to the distance of the user from the pointed target for three measurement approaches.

The comparative results of the pointing experiment for the three measuring approaches are reported in Figure 4. The figure presents the mean and standard deviation pointing accuracies with respect to the distance from the target. The overall mean errors are 491.9 mm, 333.3 mm and 157.8 mm for the FA, IF and EF, respectively. It is clear that FA measurement is the least accurate since some deviation angle at the wrist often exist. In addition, the results show that EF measurement is the most accurate while IF measurement has a somewhat larger mean error. While the EF approach is seen to be the most accurate, it exhibits several disadvantages. First, an average of 51% of individuals are more likely to exhibit congruent gaze with the target while pointing [39]. The degree of variability between individuals is high and some may settle for an implicit gaze with no observable head shift. In addition, turning the head and gazing towards the target is performed for a short period of time of approximately 670 milliseconds [40]. This is even more significant during cognitive overload where the user is performing various tasks such as during driving. Capturing the short time instant of user head-turn during pointing can be complex if it indeed occurs. Finally, having a pointing recognition model that depends both on the detection of finger and head limits the efficiency of the method in occluded environments where both must be visible. Therefore, the work in this paper is focused on the recognition of pointing solely by observing and labeling the position and direction of the index finger. Hence, the method is more robust to occlusions and user out-of-frame scenarios.

IV. METHODS

A. Problem Formulation

We consider a scenario where a user is standing in front of a mobile robot. It is assumed that the user is within the image frame of a standard RGB camera mounted on the robot. If the user is not visible, spatial voice localization can be used, for example, to attract the attention of the robot [41]. However, such a problem is not in the scope of this work. Once the user exhibits a pointing gesture, the robot is required to recognize its occurrence, estimate direction, and move towards the pointed target. A scheme for this is illustrated in Figure 2. It is important to note that pointing, in this work, is the extension of the arm along with the index finger while flexing the other fingers into the palm. While they can be included

in future efforts, we do not consider other approaches such as using more than one finger or non-manual gestures such as head movements [1].

To achieve the above goal and provide a pointing framework, we address two problems: 1) Derive a recognition model where the occurrence of a pointing gesture with the index finger is identified; and, 2) derive an estimation model for the pointing direction along with the position of the pointing finger. Images are continuously perceived by the robot in real-time. In parallel, a recognition model $h(I_t) \in \{0, 1\}$ observes image I_t at time t for whether pointing is visible $h(I_t) = 1$ or not $h(I_t) = 0$. The recognition model acts as a trigger for direction estimation and motion to the target. The estimation model $\Gamma(I_t)$, in turn, is a regression problem aimed to map image I_t to the following pointing parameters: index finger position $\mathbf{p} = (x_p, y_p, z_p) \in \mathbb{R}^3$ and pointing direction described by the pitch $\beta \in \mathbb{R}$ and yaw $\gamma \in \mathbb{R}$ angles. Pointing is, therefore, described by the feature vector $\mathbf{v} = (x_p, y_p, z_p, \beta, \gamma)$. These pointing parameters are defined relative to the coordinate frame \mathcal{O}_c of the camera as seen in Figure 5. Yaw angle γ is the rotation about the z_c axis of \mathcal{O}_c . Pitch β , on the other hand, is the angle of the finger axis with the $x_c - y_c$ plane.

Without loss of generality, we consider the problem of reaching the target goal. That is, the estimated pointing direction along with the position of the finger enable the robot to pinpoint the target location as illustrated in Figure 1. It is assumed that the user is pointing with only one arm, either right or left, while the second can do any other task. Motion planning will then be used to reach the target. In the general case and not in the scope of this work, some additional context may be required for the robot to reason about the target. For example, the user may instruct the robot to reach a door or a window. Similarly, the user can command the robot to bring a specific object. In both cases, the user will point in the corresponding direction and the robot will attempt to identify the target in the estimated direction.

B. Overview of Approach

In order to address the above objectives, we present the *PointingNet* model seen in Figure 6. *PointingNet* includes three components: *PointingNet-S* model for arm segmentation, recognition model for identifying the occurrence of pointing and *PointingNet-E* model for estimating feature vector \mathbf{v} . A user, in most cases, will be pointing in an unstructured environment with many diverse objects in the background. Hence, these objects may obscure the pointing arm and, thus, make the distinction between foreground and background objects challenging. This may be even worse as the user is farther from the camera and more objects are captured in the frame. Therefore, segmentation is the first step in order to focus the recognition and estimation models on the arm and minimize background noise. We propose to train a segmentation model *PointingNet-S* for automated masking of any lifted human arms in the frame, either pointing or not.

The segmentation is further used for pointing recognition and feature vector estimation. Segmentation can improve

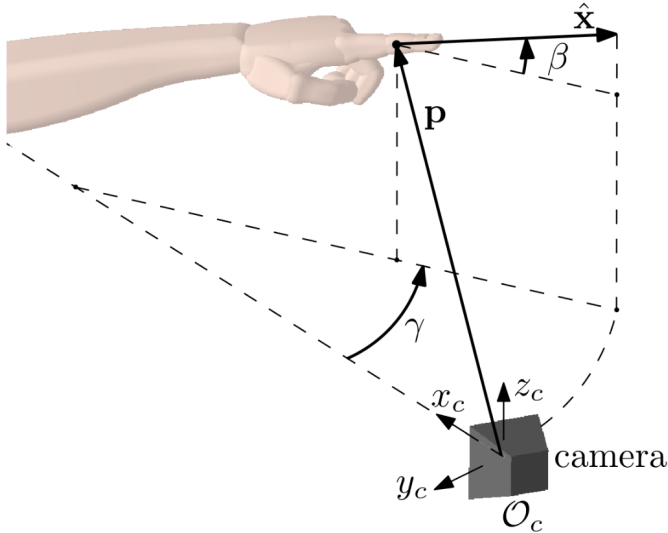


Fig. 5. Illustration of the position \mathbf{p} and direction $\hat{\mathbf{x}}$ definitions of a pointing finger with respect to the coordinate frame of the camera \mathcal{O}_c . Direction can also be represented by angles β and γ .

recognition by providing a clear and focused representation of the objects or regions of interest within an image. This allows a classifier to concentrate on the most relevant features and ignore background or irrelevant information, leading to better accuracy and reduced over-fitting. Hence, segmentation is used to crop the region of the arm and provide an input to a classification network. We note that, in preliminary study, a segmentation model was tested for only pointing arms which would obviate the need for the recognition model. However, the model provided poor results with many false negatives. Hence, a segmentation for any lifted arm followed by a recognition model provides best results.

The segmented mask is also used, along with a depth estimation of the scene, as input to the *PointingNet-E* model for estimating feature vector \mathbf{v} . We next describe the collection process of three datasets followed by a description of the segmentation, recognition and estimation models. Finally, we describe the mapping of the estimated information to robot motion to the pointed target.

C. Data Collection

To achieve the above goal, three datasets are collected for training the models. All datasets are collected by using a simple RGB camera. The first dataset \mathcal{S} is collected for training model *PointingNet-E*. A set of N_s images is collected where either the right or left arm is put in some arbitrary pose not necessarily while pointing. Consequently, the dataset is in the form $\mathcal{S} = \{I_1, \dots, I_{N_s}\}$ where I_k is an image. Similarly, dataset \mathcal{H} is collected for training the recognition model having N_h images. Each image I_i is labeled with $l_i \in \{0, 1\}$ for whether pointing is visible ($l_i = 1$) or not ($l_i = 0$). Examples of labeled images are seen in Figure 7a. Thus, the resulting data is the set $\mathcal{H} = \{(I_1, l_1), \dots, (I_{N_h}, l_{N_h})\}$.

The third dataset \mathcal{P} includes data for training the *PointingNet-E* model. While the previous two datasets are collected in various indoor and outdoor environments, the

third dataset requires a Motion Capture (MoCap) System and, therefore, collected only indoors. Nevertheless, segmentation of the arm aims to allow the model to also perform well outdoors. Each image I_j in \mathcal{P} is taken by the RGB camera and labeled using the MoCap with feature vector \mathbf{v}_j . Vector \mathbf{v}_j is obtained using a finger marker (with reflective markers as seen in Figure 7b) measured by the MoCap relative to a base marker on the RGB camera. The acquisition and labeling process yield dataset $\mathcal{P} = \{(I_1, \mathbf{v}_1), \dots, (I_{N_p}, \mathbf{v}_{N_p})\}$ of N_p samples.

In all training datasets, data is collected by several users in various distances of the user from the camera in 0.5 – 5 meters range, and in different locations within the image frame. Furthermore, we consider pointing with yaw angles in the range $\gamma \in [-125^\circ, 125^\circ]$. Angles not in the range will most likely not be visible to the robot and some intermediate pointing would have to be done to change its perspective. In order to generate a robust model, some images exhibit pointing where the user is occluded and most of the body is not visible except the pointing arm. Occlusion can occur by either an obstacle (example at the bottom of Figure 7a) or having a large portion of the user out of the image frame. In addition, pointing is performed while arbitrarily switching between right and left arms.

All images in the training dataset go through image augmentation. In addition to increasing the dataset, the augmentation encourages the model to recognize pointing in diverse and noisy environments, and also given partial information [42]. Hence, the model will be able to perform well in changing environments which include lighting variations and occlusions. Applied augmentation techniques include color jitter, random Cutout and image blur. Augmentation examples of images in the training set are seen in Figure 8.

D. Pointing Segmentation

A segmentation model breaks down an image into several segments of interests. Such process enables reducing the complexity of the problem and assists in focusing on semantically meaningful regions for further image processing. In this part, we build a segmentation model that can segment the user's arm prior to identifying if pointing occurs. For that purpose, all images in dataset \mathcal{S} are pre-processed and labeled by masking the corresponding user arm. The entire visible arm is masked including the hand and fingers. Hence, the pre-processed dataset is now $\tilde{\mathcal{S}} = \{(I_k, s_k)\}_{k=1}^{N_s}$ where s_k is the set of masked pixels in image I_k .

Using the collected data, a segmentation model termed *PointingNet-S* is proposed. First, a pre-trained Wide Residual Network (WideResNet) [43] is used with 101 layers to encode the images. WideResNet increases the width of the network, allowing it to capture complex features and patterns in the data. After encoding the image, the latent space representation is reshaped by a set of four convolutional operations, each having a different kernel. The first two kernels are odd-sized kernels of 11×1 and 1×11 . An odd-sized kernel enables centering over the input data during convolution while having rotational symmetry. The symmetry can simplify the computation and

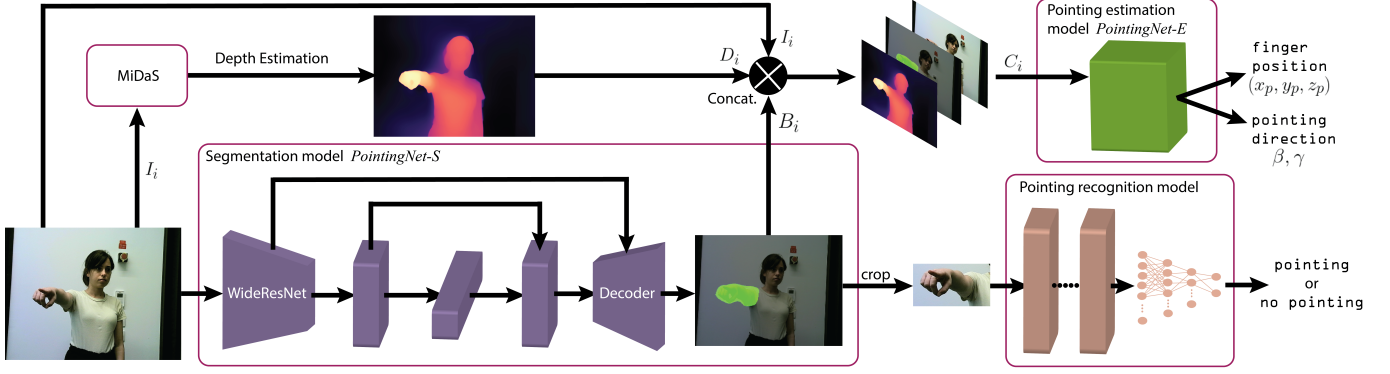


Fig. 6. Flowchart of the proposed *PointingNet* model for recognizing the event of pointing, and estimating finger position and pointing direction. A segmentation model termed *PointingNet-S* is a main component in which a mask of a lifted arm is outputted. Then, the cropped arm image is passed through a CNN for classification of whether pointing is visible. If pointing is indeed identified, estimation model *PointingNet-E* is triggered where its input is the concatenation of the original image, the masked image and an estimated depth image generated by MiDaS. The output of the estimation model is the position of the finger and direction of pointing, both with respect to the coordinate frame of the camera.

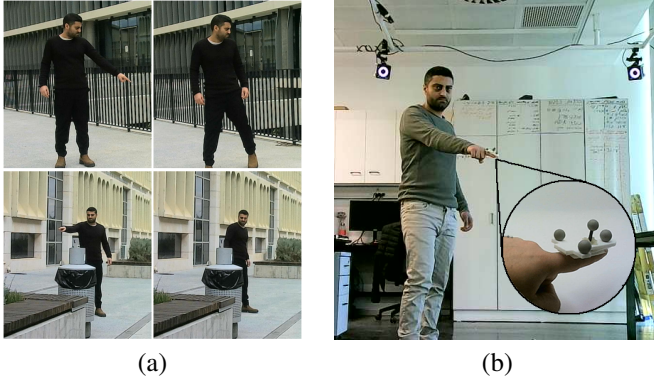


Fig. 7. Data collection for (a) recognition model by labeling images with pointing (left) or not pointing (right), and (b) estimation model by labeling images with a motion capture system observing a finger marker relative to a camera marker.

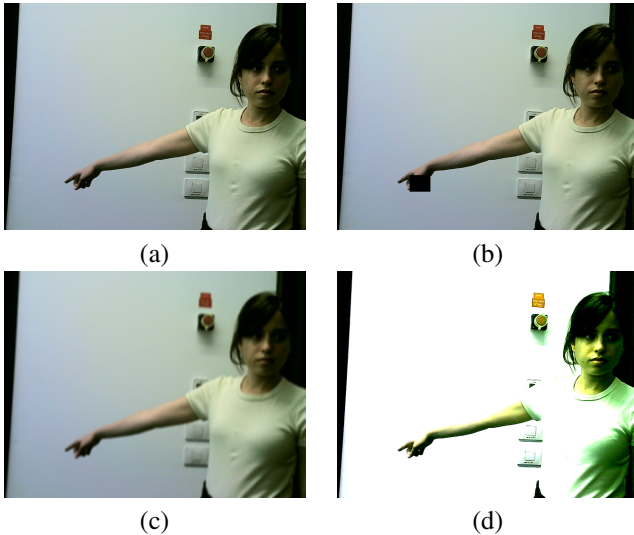


Fig. 8. Augmentation examples of images in the training data: (a) original image, (b) random cut-out from image (black rectangle on hand), (c) image blur and (d) color jitter.

make the network more robust to rotational variations in the input data. Two additional convolutions are Atrous with a rate of two and three. The Atrous convolution dilates the window size while incorporating gaps between data values so to increase the field of view without increasing the number of weights. Finally, the four convolutions are concatenated and fed into a standard decoder comprising 48 convolutional layers. In addition, skip connections are added between the encoder and decoder and between the convolutions to avoid overfitting, improve gradient flow and encourage the reuse of features. The model is trained with dataset \tilde{S} and a Binary Cross-Entropy (BCE) with logits loss. The segmentation model is illustrated in Figure 6. In conclusion, we acquire a segmentation model $\hat{s}_i = S(I_i)$ that outputs the predicted set of pixels \hat{s}_i masking any lifted arm in image I_i .

E. Pointing Recognition

Object recognition refers to techniques or algorithms for recognizing objects within images. Neural-networks, which are trained to recognize patterns in data, are efficient for such tasks and include techniques of classification, detection and segmentation [44], [45]. In our pointing recognition problem, the task involves identifying whether the user seen in a query image exhibits a pointing gesture. In order to eliminate background noise and interferences, the *PointingNet-S* model described above is used to detect any lifted arm in the image, crop out the rest of the image and proceed to further classification. Therefore, dataset \mathcal{H} is pre-processed to include only cropped images of lifted arms. That is, each image $I_i \in \mathcal{H}$ is passed through the segmentation model and cropped to the minimal area rectangle bounding predicted label $\hat{s}_i = S(I_i)$. The pre-processed dataset $\tilde{\mathcal{H}} = \{(\tilde{I}_i, l_i)\}_{i=1}^{N_h}$ is acquired where \tilde{I}_i is the cropped image of I_i .

Using $\tilde{\mathcal{H}}$, a recognition model $h(I_i)$ is trained for binary classification of images. Specifically, the model would determine whether an arm seen in an inputted cropped image exhibits pointing or not. Various classification models can be used to solve the pointing recognition task. Comparative analysis to be presented in the evaluation section show that

marginal performance differences exist between a simple NN models (e.g., Fully-Connected NN or Convolutional-NN) to more complex pre-trained models (e.g., GoogLeNet [45]). In addition, the former provides lower-computational costs and more suitable for real-time predictions. Therefore, we propose the use of a Convolutional NN (CNN) architecture with four convolutional layers. The output of the final convolutional layer is flattened and fed into a series of eight fully-connected (FC) layers used for binary classification. The output of the final FC layer is passed through a Sigmoid activation function in order to obtain a predicted probability for whether the input image exhibits pointing.

F. Pointing Estimation

Once a pointing gesture has been recognized, the pointing feature vector \mathbf{v} is to be estimated. As discussed in Section I, common approaches for human pose estimation are based on learning keypoints on the human body forming a skeletal representation (e.g., MediaPipe [46] and VNect [22]). As will be shown in the Evaluation Section, computing either forearm [18], [27] or index finger direction from these keypoints results in poor estimation accuracy. In addition, these keypoints are measured with respect to some arbitrary coordinate frame and not relative to the camera. Hence, state-of-the-art human pose estimation approaches cannot be used to extract the position of the pointing finger.

The prominent disadvantage of using regular RGB images is the lack of spatial information and, in particular, the user's 3D pose relative to the camera. Therefore, we incorporate the MiDaS Monocular Depth Estimation model [47], [48] which adds depth information to the observed RGB image. MiDaS uses a single monocular camera to estimate the depth of objects in the scene with respect to the camera. Hence, each image $I_j \in \mathcal{P}$ is passed through the MiDaS model to generate a corresponding RGB depth image D_j . Furthermore, arm segmentation can focus the model on regions of interest. Hence, the predicted mask $\hat{s}_j = S(I_j)$ is used to generate a binary image B_j (i.e., white and black for arm and non-arm regions, respectively). Finally, the images I_j , D_j and B_j are concatenated to a seven-channel image C_j . This configuration enables to observe spatial relations, to omit irrelevant features and to lower the required amount of data for training the pointing estimation model. While the full arm is segmented, the label for training *PointingNet-E* is the direction of the index finger. The index finger is included in the segmented arm. Also, the model receives additional information in the image, both in I_j and D_j , including the standing pose of the human body with approximated depth information. Therefore, the model can learn dependencies of body and arm postures to the direction of index finger.

The proposed *PointingNet-E* for pointing estimation encodes the multi-channel image C_j to acquire an estimated feature vector $\tilde{\mathbf{v}}_j = \Gamma(C_j)$. *PointingNet-E* is based on an eight-layers ConvNeXt encoder [49]. The key innovation of ConvNeXt is its use of channel groups within the network for efficient capturing of diverse features in input images. By combining different types of convolutions within a block,

ConvNeXt can capture both low-level and high-level features while maintaining a low computational cost. We modify the ConvNeXt to include skip-connections. That is, the output of layer i is passed to layer $i + 1$ and also concatenated with the output of layer $i + 2$ after down-sampling. These multiple pathways provide a form of redundancy that enables advanced information sharing and makes the network more robust to noisy or incomplete data.

The output of the ConvNeXt encoder is further passed through three different Fully-Connected Neural-Network (FC-NN) blocks. Preliminary results have shown that it is significantly more accurate to estimate each feature in pointing vector \mathbf{v}_i with a designated FC-NN rather than with a single FC-NN for all features. Hence, each of the three FC-NN blocks outputs either angle β_i , angle γ_i or position \mathbf{p}_i of pointing feature vector \mathbf{v}_i . All FC-NN's consist of four FC layers having Rectifier Linear Unit (ReLU) activation functions in between. However, only the FC-NN's of the angles have a Sigmoid activation function at the output. The model is trained to minimize a loss function summing the Root Mean Square Error (RMSE) and Mean Squared Error (MSE) of the angles and position, respectively, over dataset \mathcal{P} . In conclusion, given an image I_j with exhibited pointing, depth estimation D_j and binary arm mask B_j are extracted so to estimate the feature vector $\tilde{\mathbf{v}}_j = \Gamma(C_j)$.

G. Robot motion

In the idling state, the robot will loop through a stream of real-time images acquired from the camera. The images will pass through the pointing recognition model h . Once a pointing gesture is identified, the estimation model Γ is triggered to output an estimated feature vector $\tilde{\mathbf{v}}$. Hence, the estimated position of the finger $\tilde{\mathbf{p}}^{(c)}$ and direction angles $\tilde{\beta}, \tilde{\gamma}$ are now known. The superscript $(\cdot)^{(c)}$ indicates coordinates with respect to the frame \mathcal{O}_c of the camera. The unit vector $\hat{\mathbf{x}}^{(c)}$ in the direction of pointing is acquired by

$$\hat{\mathbf{x}}^{(c)} = \begin{pmatrix} \cos \tilde{\gamma} \cos \tilde{\beta} \\ \sin \tilde{\gamma} \cos \tilde{\beta} \\ -\sin \tilde{\beta} \end{pmatrix}. \quad (2)$$

Given the homogeneous transformation matrix $A_{r,c} \in SE(3)$ mapping from \mathcal{O}_c to the robot coordinate frame \mathcal{O}_r , finger position and pointing direction are expressed in \mathcal{O}_r according to

$$\begin{pmatrix} \hat{\mathbf{x}}^{(r)} \\ 1 \end{pmatrix} = A_{r,c} \begin{pmatrix} \hat{\mathbf{x}}^{(c)} \\ 1 \end{pmatrix} \quad (3)$$

and

$$\begin{pmatrix} \tilde{\mathbf{p}}^{(r)} \\ 1 \end{pmatrix} = A_{r,c} \begin{pmatrix} \tilde{\mathbf{p}}^{(c)} \\ 1 \end{pmatrix}. \quad (4)$$

Furthermore, it is assumed that the environment of the robot is fully known such that distance d from the finger to the floor plane along vector $\hat{\mathbf{x}}^{(r)}$ can be estimated. For instance, if both user and robot are on a flat horizontal floor, distance d can be calculated according to simple proportionality

$$d = -\frac{\tilde{p}_z^{(r)} + h}{\hat{x}_z^{(r)}} \quad (5)$$

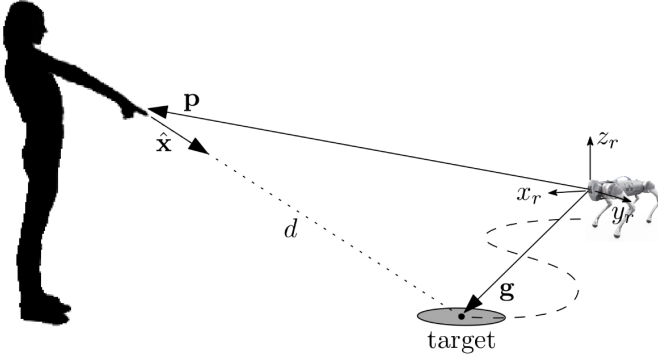


Fig. 9. Once the target \mathbf{g} is computed, the robot can plan and control the motion to it (dashed curve). All vectors are expressed in the coordinate frame of the robot \mathcal{O}_r after mapping from frame \mathcal{O}_c .

where $\tilde{p}_z^{(r)}$ and $\hat{x}_z^{(r)}$ are the z components of $\tilde{\mathbf{p}}^{(c)}$ and $\hat{\mathbf{x}}^{(r)}$, respectively, and h is the height of the robot. Generally, the target location \mathbf{g} in \mathcal{O}_r for the robot to reach is acquired according to the resultant vector

$$\mathbf{g} = \tilde{\mathbf{p}}^{(r)} + \hat{\mathbf{x}}^{(r)}d \quad (6)$$

as seen in Figure 9. Once the target has been identified, the robot can walk directly to it if the environment is known to be obstacle-free. Alternatively, the robot can apply some motion planning algorithm [50] to plan a more complex path considering obstacles in the environment.

V. MODEL EVALUATION

This section tests and analyzes the proposed *PointingNet* model including analysis of arm segmentation, recognition model for classifying occurrences of pointing and direction estimation. We describe the collection of training and test data followed by an analysis of the model components. All model training and evaluations were performed on a Linux Ubuntu (18.04 LTS) machine with Intel Xeon Gold 6230R (20 Cores of 2.1GHz) CPU and four NVIDIA GeForce RTX 2080TI GPU (11GB of RAM). Neural-Network models were trained and tested using PyTorch. Videos of the data collection, experiments and demonstrations can be seen in the supplementary material.

A. Database and Descriptors

As discussed in Section IV-C, three datasets \mathcal{S} , \mathcal{H} and \mathcal{P} were collected for arm segmentation, pointing recognition and pointing direction estimation, respectively. For the collection of these datasets, 12 participants were recruited where nine and three participants contributed training and test data, respectively. Participants and recorded environments in the test set were not included in the collection of training data. Participants include four females and eight males with maximum and minimum heights of 1.56 m and 1.91 m, respectively. All image data was collected with a simple web-camera yielding images of size 480×640 . However, in order to enable robust usage with any camera, the images were reduced to resolution 288×384 . To enhance the labeling process of the information, the acquired data for segmentation was obtained

at a resolution of 1920×1080 and later reduced. This allows for a more comprehensive visualization of objects or regions of interest and facilitates the identification and annotation of such elements.

Both datasets \mathcal{S} and \mathcal{H} were collected by the participants in indoor and outdoor environments. Participants stood in various locations in-front of the camera and up to five meters from it. During recording, no other participant was visible in the image. Each participant was asked to randomly point at any desired direction with a sole constraint of pointing within the range of $\gamma \in [-125^\circ, 125^\circ]$. Participants arbitrarily switched between their right and left arm. Also, participants arbitrarily chose to have short or long sleeves during recording. The collection yielded $N_s = 17,698$ and 1,800 train and test samples, respectively, for dataset \mathcal{S} . In addition to many images of pointing, the dataset includes images of lifted arms in various tasks such as waving or holding an object. To allow for robust segmentation models, some images included scenarios without any participant or with features resembling a human arm (e.g., unused coat or shirt). These images were given a blank mask (i.e., no segmentation). To generate the masked dataset $\tilde{\mathcal{S}}$, images in \mathcal{S} were pre-processed and labeled by masking the corresponding user arm with the *V7 auto-annotate* tool.

Dataset \mathcal{H} for classification includes $N_h = 20,000$ training samples and 2,000 test samples. Half of \mathcal{H} is of participants exhibiting pointing in the images and labeled $l_i = 1$. Images of the other half, labeled $l_i = 0$, include participants doing various tasks while standing, walking, sitting or crouching but without pointing. The third data set \mathcal{P} includes $N_p = 186,300$ and 17,458 train and test samples, respectively, of images labeled with pointing feature vectors. Feature vector \mathbf{v}_i was measured by a MoCap system with eight OptiTrack Prime 41 cameras as discussed in Section IV-C and demonstrated in Figure 7b. Since a MoCap was used, the collection was only performed indoors.

B. PointingNet-S evaluation

As discussed in Section IV-D, segmentation focuses the recognition and estimation models on the user's arm. *PointingNet-S* is a designated model for segmentation of lifted arms in images. We compare *PointingNet-S* to various state-of-the-art segmentation models including Autoencoder, U-Net, U-Net++, Feature Pyramid Network (FPN), ResNet-101, DenseNet and DeepLabV3+. The baseline is a simple Autoencoder in which the original image is encoded and reconstructed to the masked variant [51]. U-Net is a widely used image segmentation model for biomedical applications where the image is contracted and expanded in a U shaped path of convolutional layers [52]. U-Net++ is an extension of the U-Net architecture with additional skip-connections to improve segmentation accuracy [53]. Similarly, FPN uses a pyramid-shaped feature hierarchy to extract features at different scales for object segmentation [54]. ResNet-101 [55] and DenseNet-201 [56] are deep learning models that use residual connections and densely connected blocks, respectively, to improve accuracy and reduce overfitting. DeepLabV3+ model

TABLE II
ARM SEGMENTATION EVALUATION RESULTS

Models	IoU
Autoencoder	66.9%
U-Net	60.1%
U-Net++	86.6%
FPN	69.2%
ResNet-101	78.5%
DenseNet-201	82.9%
DeepLabV3+	86.1%
<i>PointingNet-S</i>	94.3%



Fig. 10. Arm segmentation examples outputted by *PointingNet-S* in various scenarios of multiple participants, occlusions, dual-arm lift, sitting down and holding objects. The segmentation is performed for any lifted arm regardless of pointing or not. Classification later determines if pointing indeed occurs.

uses dilated convolution and an encoder-decoder structure with a ResNet-101 backbone to preserve fine details [57]. These models are commonly used to identify and segment various objects in images in different applications. They provide different trade-offs between accuracy and computational efficiency. Hence, the comparison is important since the performance of the models vary based on the specific segmentation task and dataset.

All evaluated models are trained with dataset \tilde{S} and evaluated on the independent test set. The performances of all models are evaluated with the Intersection over Union (IoU). IoU calculates the percentage ratio between overlapping and unified areas of the ground-truth and predicted masks. Table II reports the comparative IoU results between all methods. While some models achieved adequate accuracy, *PointingNet-S* is shown to provide superior results by a large margin. Figure 10 shows examples of predicted segmentation of the arms in various scenarios. *PointingNet-S* is able to segment lifted arms in complex scenarios including multiple users in the frame, occlusions and user pointing while body is out-of-frame.

C. Pointing Recognition Evaluation

Once segmentation of the arm has been acquired, the image is cropped to include only the arm. As discussed in Section IV-E, the cropped image is passed through the

TABLE III
POINTING RECOGNITION EVALUATION RESULTS

Models	Segmentation	
	w/o	w/
FC-NN	-	96.6%
CNN	66.7%	97.2%
ResNet-18	74.6%	98.1%
VGG-19	75.1%	98.5%
GoogLeNet	78.9%	98.7%

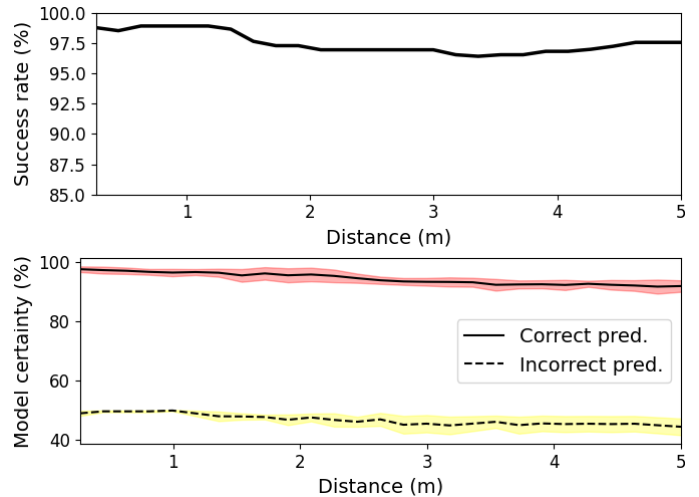


Fig. 11. Classification (top) success rate and (bottom) certainty with regards to the distance of the user's arm from the camera.

classification model in order to determine if pointing occurs. In our proposed approach, a CNN network is trained to perform the classification. We compare the model with various other models including FC-NN, ResNet-18, Visual Geometry Group (VGG) and GoogLeNet. VGG is a popular model for object recognition and segmentation that uses a deep convolutional architecture [58]. Similarly, GoogLeNet is a deep CNN having a unique inception module that incorporates multiple filters in parallel [45]. In addition, we compare classification with and without segmentation of the arm. When not including segmentation, the entire image is passed through the model.

Table III reports classification success rate for all models with and without segmentation. First, not using segmentation exhibits poor results and validates the need to focus the model on the arm. In addition, the results with segmentation show marginal differences between simple models, such as FC-NN and CNN, to the more complex models with advantage to the latter. However, the marginal improvement may not justify the significant increase in computational cost of runtime and memory usage. Hence, we use the proposed CNN for further experiments while more complex models are optional.

Figure 11 reports the classification success rate and certainty with regards to the users distance from the camera. The success rate and model certainty for correct predictions are stable and high. However, certainty for incorrect predictions is low. Hence, one can identify and ignore erroneous ones.

D. PointingNet-E Evaluation

Once pointing is identified, *PointingNet-E* is triggered. In this section, we evaluate the performance of the model on the

TABLE IV
POINTING DIRECTION ESTIMATION RESULTS

		Position RMSE (mm)	Yaw MAE ($^{\circ}$)	Pitch MAE ($^{\circ}$)
MediaPipe	(index finger)	-	26.1 \pm 12.2	17.3 \pm 16.0
	(forearm)	-	29.6 \pm 10.7	15.8 \pm 12.5
VNect	(forearm)	-	46.8 \pm 26.3	30.5 \pm 17.4
OpenPose	(forearm)	-	33.7 \pm 26.3	16.6 \pm 10.6
CNN		241.1 \pm 8.1	41.2 \pm 8.3	44.3 \pm 21.2
VGG-19		95.4 \pm 4.7	29.1 \pm 7.8	40.4 \pm 19.7
DenseNet		162.8 \pm 79.4	21.9 \pm 10.1	13.5 \pm 4.5
<i>PointingNet-E</i>	I_i only	216.5 \pm 55.1	38.2 \pm 6.7	17.9 \pm 7.7
<i>PointingNet-E</i>	I_i & D_i	94.3 \pm 4.18	7.17 \pm 6.1	3.43 \pm 2.4
<i>PointingNet-E</i>	I_i & B_i	77.1 \pm 84.7	8.4 \pm 3.6	7.8 \pm 6.3
<i>PointingNet-E</i>	C_i	61.3 \pm 30	1.4 \pm 1.3	0.61 \pm 0.63

test data and in real-time predictions. *PointingNet-E* model was trained with dataset \mathcal{P} as discussed in Section IV-F. Accuracy of the model over the test data is evaluated using Root Mean Square Error (RMSE) for the finger position and Mean Absolute Error (MAE) for yaw and pitch angles, all with respect to the measured ground-truth.

Table IV presents an overall comparison of the proposed approach with various known models. First, we evaluate the pointing accuracy with state-of-the-art skeleton-based human pose estimation models including MediaPipe [21], VNect [22] and OpenPose [20]. These models are pre-trained and used as provided through open-source distribution. While VNect and OpenPose offer spatial pose estimation of only the forearm, MediaPipe can provide spatial estimation of the finger as well. Hence, pointing is evaluated solely using forearm keypoints for the former two while using also the index finger for the latter. Human pose estimation models are not trained nor designated for the pointing estimation problem. Therefore, all results with these models yield poor direction accuracy. We note also that the position of the finger is given with respect to some unknown coordinate frame and cannot be transferred to the camera’s coordinate frame as required. Hence, skeleton-based human pose estimation models are shown to be inadequate for pointing applications and cannot be used in practice for directing robots.

The proposed model is next compared to various deep NN models including a simple CNN, VGG-19 and DenseNet. The input for these models is only the original image I_i . Furthermore, *PointingNet-E* is benchmarked across different inputs: only the original image I_i ; a concatenation of I_i with the MiDaS depth approximation D_i ; a concatenation of I_i with arm mask B_i ; and, the concatenation C_i of all three I_i , B_i and D_i . The results in Table IV show poor accuracy for CNN, VGG-19 and DenseNet as well as for *PointingNet* with only I_i , both in position and direction. However, including B_i or D_i to I_i significantly reduces estimation errors. These results, therefore, highlight the importance of each of the three components in predicting the position and direction of pointing gestures. Consequently, having all three images I_i , B_i and D_i provides significantly lower position and direction errors (less than 2° in average). Figure 12 shows *PointingNet-E* estimation accuracy with regards to distance of the user from the camera. Results show slight error increase with distance while still being fairly accurate. In addition, Figures 13 and

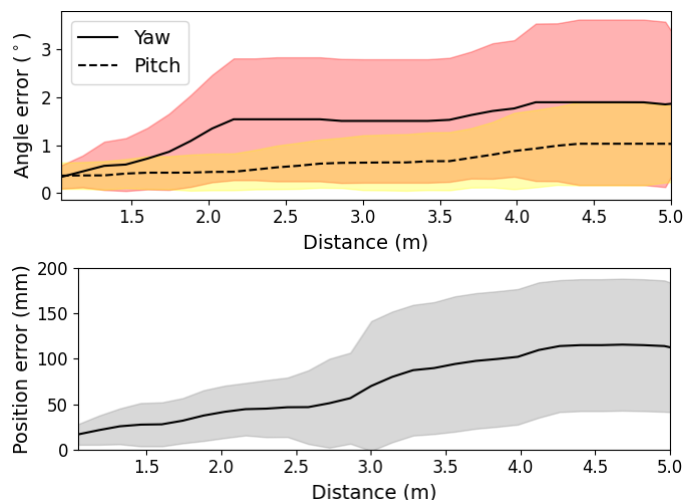


Fig. 12. Prediction errors of (top) yaw and pitch angles and (bottom) position with regards to the distance of the user’s arm from the camera.

14 show the prediction errors of the yaw and pitch angles, respectively, with respect to the angles themselves. The plots show relatively uniform error distribution across the learned range. These results validate the effectiveness and feasibility of *PointingNet-E* for accurate estimation of pointing.

Heatmaps of yaw, pitch and position estimation errors with respect to data sizes can be seen in Figures 15-17. The errors are calculated over the test data while increasing the number of points N_p in \mathcal{P} for *PointingNet-E* and the number of points N_s in \mathcal{S} for *PointingNet-S*. For each cell in the heatmap, *PointingNet-S* was trained with N_s training data and then used to segment N_p data for training *PointingNet-E*. The figures also show curves for the error during the increase of training data for *PointingNet-E* while having *PointingNet-S* trained with all available data. The accuracy increases with the addition of pointing examples. In addition, the results show the importance of a sufficiently trained segmentation model which also emphasize the contribution of arm segmentation to the pointing estimation accuracy.

Figure 18 shows an example for one pointing test image inputted to *PointingNet-E* and the images extracted from its layers. The initial layers of the modified ConvNeXt predominantly detect the edges of the image with a some focus on the arm. In the following layers, there is a stronger emphasis on the region of interest, i.e., the arm, compared to the background areas. The output of the fifth layer highlights the pose of the arm. In the final layers, the model prioritizes the finger and the entire arm region receiving the highest intensity. While it is hard to reason about the exact features learned by the model, visualization of the learned features in each layer of *PointingNet-E* provides implications that the model learns to distinguish between the different elements of the image and focuses on arm and finger posture. Presumably, *PointingNet-E* learns to predict finger position and direction by observing the index finger, but based also on learning patterns of arm postures.

Next, the ability of the model to provide pointing position and direction estimation in real-time is demonstrated. Here,

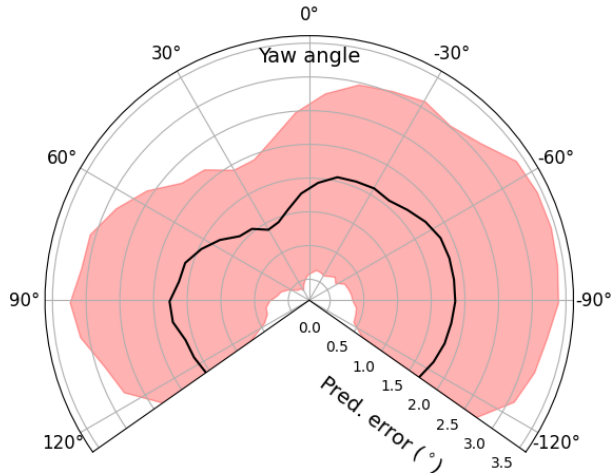


Fig. 13. Prediction error distribution of the yaw γ angle.

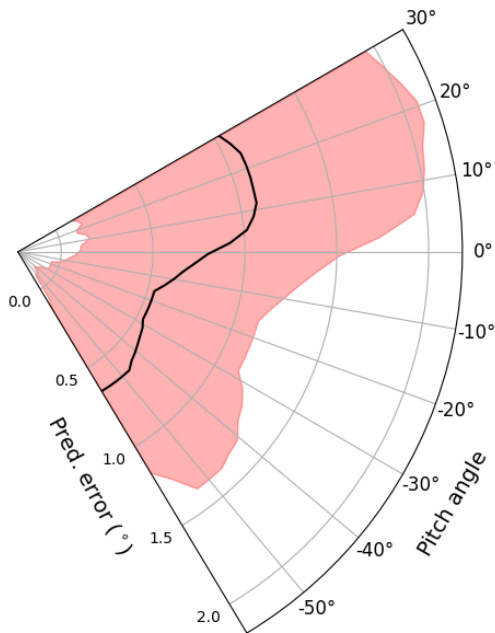


Fig. 14. Prediction error distribution of the pitch β angle.

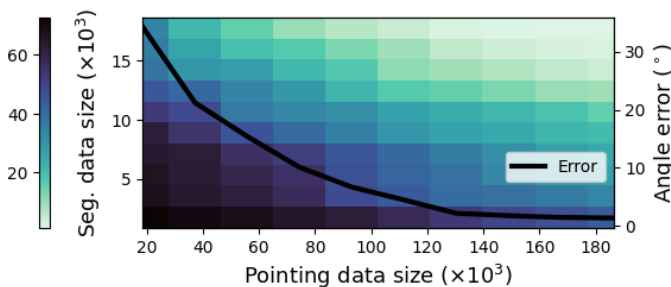


Fig. 15. Heatmap of the yaw angle error ($^{\circ}$) with regards to the sizes of \mathcal{P} and \mathcal{S} to train *PointingNet-E* and *PointingNet-S*, respectively. The black curve (with the right y -axis) shows the error of the yaw angle estimation with *PointingNet-E* when using the fully trained *PointingNet-S*.

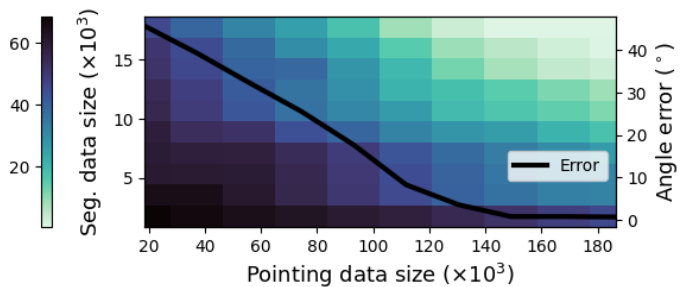


Fig. 16. Heatmap of the pitch angle error ($^{\circ}$) with regards to the sizes of \mathcal{P} and \mathcal{S} to train *PointingNet-E* and *PointingNet-S*, respectively. The black curve (with the right y -axis) shows the error of the pitch angle estimation with *PointingNet-E* when using the fully trained *PointingNet-S*.

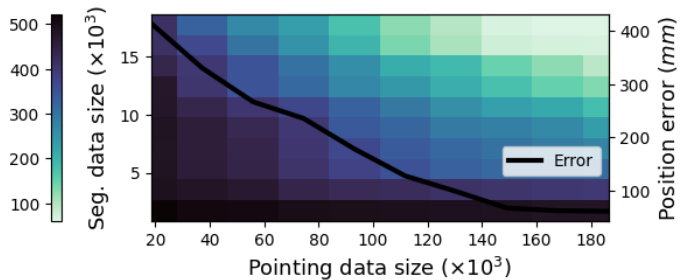


Fig. 17. Heatmap of the position error (mm) with regards to the sizes of \mathcal{P} and \mathcal{S} to train *PointingNet-E* and *PointingNet-S*, respectively. The black curve (with the right y -axis) shows the error of the position estimation with *PointingNet-E* when using the fully trained *PointingNet-S*.

the test participant moved the arm fairly slow while changing pointing directions. The camera acquired images in frequency of 38 Hz. Prediction accuracy matches the ones reported in Table IV. Furthermore, Figure 19 shows an example of one real-time prediction session. The mean yaw and pitch angles along the session are 1.78° and 0.8° , respectively. Similarly, the position errors along the x -, y - and z -directions are 102.7 mm, 20.66 mm and 21.83 mm, respectively. *PointingNet-E* predictions closely match the ground-truth with slightly larger errors along the x -axis. Overall, the results provide strong evidence that our model is able to accurately predict the direction and position of pointing gestures in real-time.

E. Edge Cases

We next evaluate the performance of *PointingNet* in specific but interesting edge cases where accurate predictions may

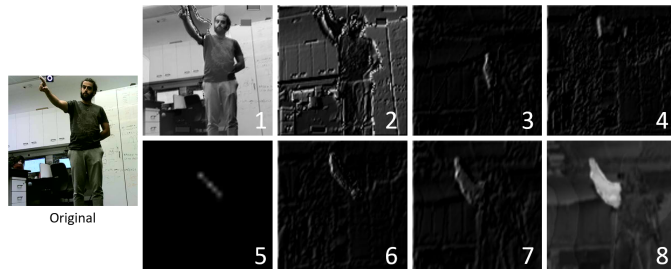


Fig. 18. Original image (left) of a pointing participant and the outputted images from the first (1) to last (2) layers of the ConvNeXt in *PointingNet-E*.

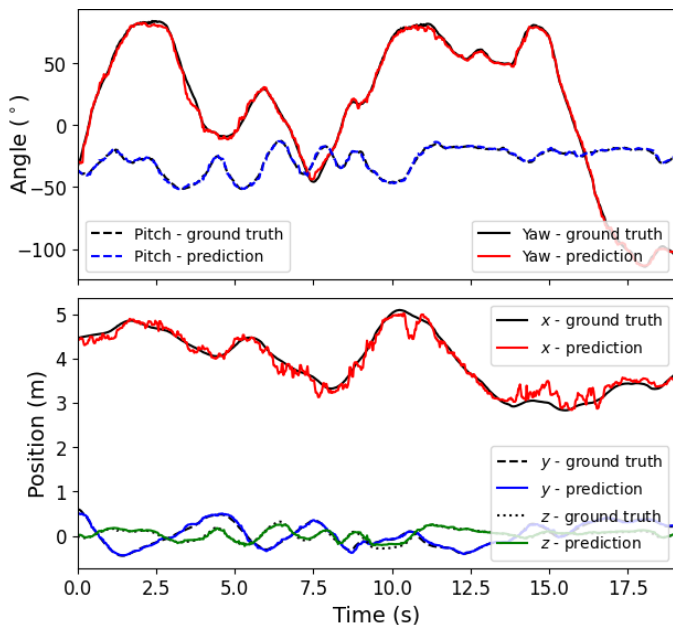


Fig. 19. Real-time prediction of pointing parameters including (top) yaw and pitch angles and (bottom) position of the user’s finger.

be difficult. Note that previous experiments included these edge cases in the test data. However, we provide a designated analysis in this section to better emphasize the abilities of *PointingNet*. Designated test sets were collected for six edge cases including: gloved hands, out-of-frame participant, partly occluded participant, multi-users in the image, pointing while seated and dual-arm lift.

In the gloved hands case, participants pointed while wearing blue or black surgical gloves (Figure 20a). This also evaluates model robustness to skin color. In the out-of-frame case, participants were positioned outside the camera’s frame with only their pointing arm visible (Figure 20b). This demonstrates the independence of the model from other body parts as required in other methods. Similarly, during occlusion, part of the participants body is not visible. Hence, the participants stood behind large objects (e.g. a chair and a ladder) with their bodies partially occluded while their pointing arms are clearly visible (Figure 20c). In multi-user cases, several participants are seen in the image while only one is pointing (Figure 20d). We do not consider cases where more than one participant is pointing. In the fifth case, participants pointed while sitting down (Figure 20e). Finally, the dual-arm case involves participants lifting both arms (Figure 20f) while one is pointing and the other is performing other tasks (e.g. head scratching or waving). All test sets were collected and labeled as described previously.

Table V summarizes the classification success rate and pointing estimation for all six edge cases. The success rate remains high with a slight decrease for occlusions, multi-users and dual-arm. Occlusions and out-of-frame are relatively similar scenarios. However, the arm in out-of-frame scenarios is in the foreground and clearly visible. In occlusions, on the other hand, the arm is in the background while foreground objects have the focus. This is likely why occlusion images

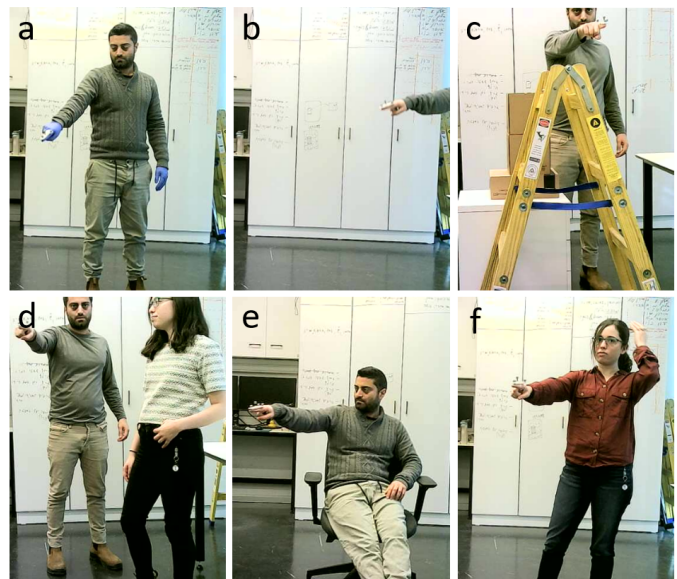


Fig. 20. Examples of the six evaluated pointing edge cases: (a) user wearing gloves, (b) user is out-of-frame and only the pointing arm is visible, (c) user is partly occluded by objects in the scene, (d) multiple people in the scene where the pointing user is in the background, (e) user is sitting down and, (f) both arms of the user are lifted.

TABLE V
RECOGNITION SUCCESS RATE AND ESTIMATION ACCURACY FOR SEVERAL EDGE CASES

	Success (%)	Position (mm)	Pitch (°)	Yaw (°)
Gloves	94.9	81.3±44.0	10.89±6.9	11.02±3.2
Out-of-frame	95.5	75.5±35.8	10.22±3.7	12.44±6.1
Occlusions	89.5	70.9±29.6	11.75±5.9	12.86±3.7
Multi-users	90.5	72.3±34.1	6.57±2.98	7.43±4.54
Sitting-down	97.9	68.8±35.6	3.87±1.88	5.08±2.12
Dual-arm	87.8	70.1±38.8	7.45±2.61	8.03±2.94

receive lower success rate.

When comparing pointing estimation with the general error, positional errors negligibly increase by 11 mm on average. However, the yaw and pitch errors increase by an average of 8.08° and 7.84°, respectively. Estimating pointing direction in these cases is somewhat harder and the mean errors are larger compared to the general error. Nevertheless, these errors remain low and feasible for accurate pointing. One may improve accuracy in these cases by adding corresponding image samples to the training data.

VI. ROBOT EXPERIMENTS

Following the evaluation of *PointingNet*, the effectiveness and practicality of the model is experimented over robotic platforms in pointing-based human guidance. The user’s ability to guide the robot towards a desired goal is an essential aspect of HRI, as it involves direct communication and coordination between the human and the robot. The following experiments provide an assessment of the model’s feasibility for real-world applications over two different robotic platforms. The experimental setups are first described followed by results.

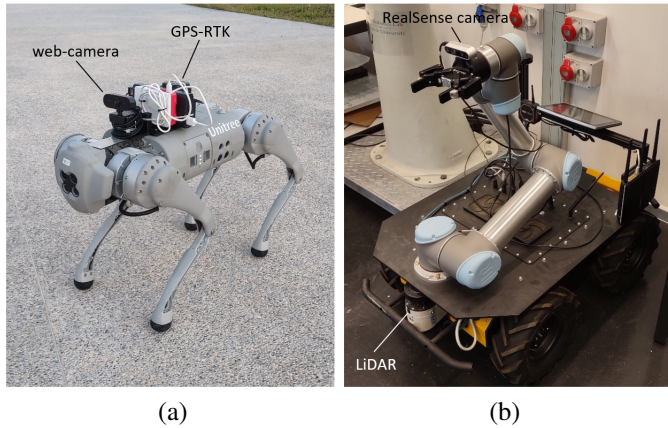


Fig. 21. Two robotic platforms used in the experiments: (a) Unitree Go1 quadruped robot equipped with a simple RGB web camera for pointing recognition and a GPS-RTK for localization. (b) Clearpath Husky 4-wheel rover equipped with a RealSense camera (only RGB data is used) for pointing recognition and a 2D LiDAR for localization.

A. Setup

1) *Software*: The *PointingNet* model was wrapped into a Robot Operating System (ROS) node. Hence, the framework described in Figure 2 is implemented in ROS and predicts pointing in real-time. The recognition model, with internal *PointingNet-S* segmentation, loops until pointing is identified. Once identified, the estimation model *PointingNet-E* is triggered to predict feature vector \mathbf{v} that corresponds to the captured image. In practice, ROS loops for several more images after the trigger in order for the pointing arm to complete its motion and become static. In our experiments, we assume a flat horizontal floor. Hence, the pointed target is approximated according to (5)-(6). The target is then transferred to a planning and control node which is implemented individually for each of the two robotic platforms described next. In both platforms, however, real-time calculations are performed over a central computer where WiFi communication enables bi-directional transfer of sensed information and motion commands.

2) *Go1 quadruped robot*: The first platform is the Unitree Go1 quadruped robot seen in Figure 21a. A web camera was mounted on top of the robot in order to observe pointing users. Furthermore, a GPS-RTK board and an Inertial Measurement Unit (IMU) are used for global localization and heading calculations, respectively. The robot is controlled using the manufacturer’s high-level ROS API. Hence, the planning and control node commands the robot to move directly towards the target location and stop once reached. The experimental trials were conducted in an open environment without any obstacles.

3) *Husky Rover*: The second platform is the Husky 4-wheel rover by Clearpath. The rover is equipped with a Sick 2D LiDAR for localization. Hence, prior to the experiments, the robot mapped the environment in order to localize itself such that it is able to pin-point any pointed target within the generated map. To demonstrate the ability of *PointingNet* to acquire images from various cameras, a RealSense RGB-Depth camera was mounted on the robot as seen in Figure 21b. Nevertheless, only RGB data was obtained from the camera. When experimenting with the rover, the pitch angle

TABLE VI
EXPERIMENTAL RESULTS FOR ROBOT REACHING TO POINTED TARGETS

System	Success rate (%)	Target reach error (m)	Distance to target (m)
Quadruped	100	0.36 ± 0.28	3.8 ± 0.95
Rover	86.7	0.32 ± 0.2	7.2 ± 2.5

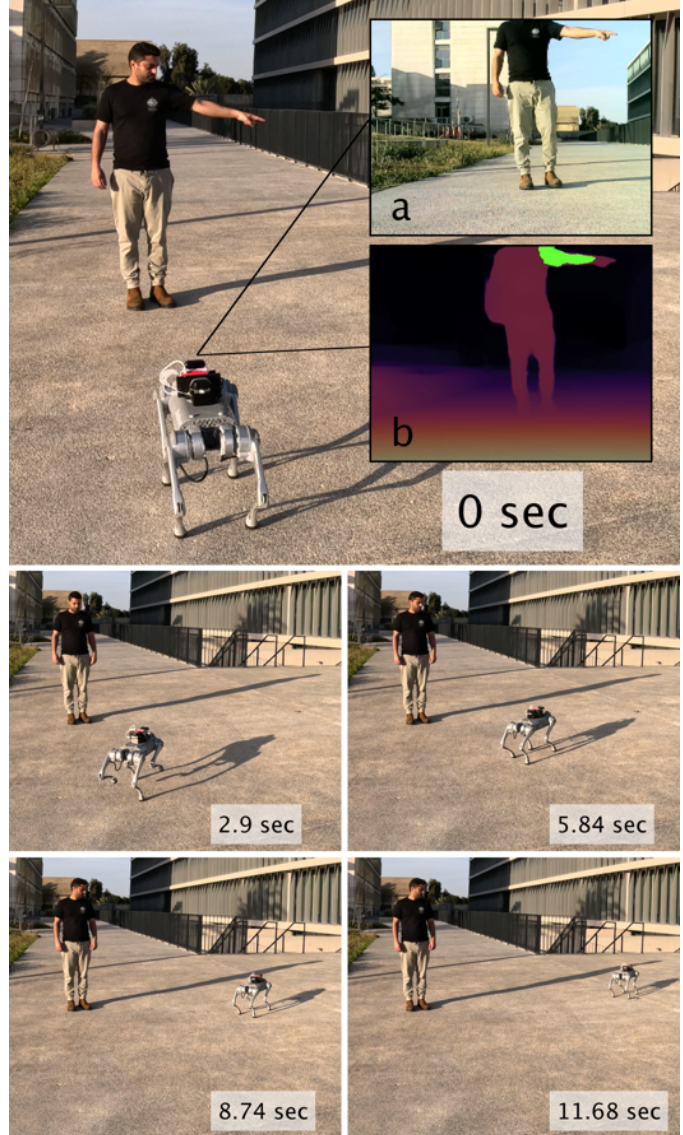


Fig. 22. Snapshots of a pointing experiment with the quadruped robot. The top image shows the moment of pointing along with (a) the image observed by the robot and (b) estimation of pointing direction. The robot reached the target with an accuracy of 0.07 m.

was ignored. Hence, the robot is instructed to move along a line formed by the projection of the pointed vector on the floor starting from the position of the finger. The ROS node for planning and control will direct the robot to reach the start of the projected line and move along it until encountering an obstacle. In the experimental trials, a small bench was set as the desired target such that the robot can identify it as an obstacle and stop in front of it.

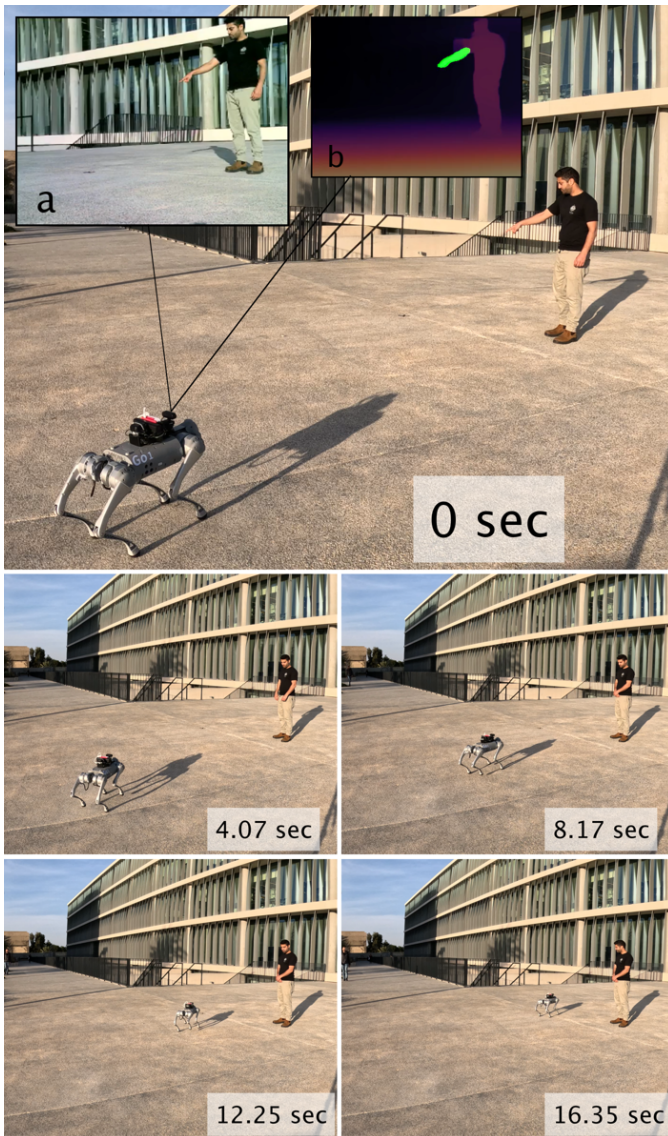


Fig. 23. Snapshots of a pointing experiment with the quadruped robot. The top image shows the moment of pointing along with (a) the image observed by the robot and (b) estimation of pointing direction. The robot reached the target with an accuracy of 0.13 m.

B. Results

A set of experimental trials was conducted for each of the robot platforms. Each set included 15 pointing trials to arbitrary targets with respect to the user and robot. In each trial, the user and robot were randomly re-located such that the user stood in front of the robot in a random relative distance. For the quadruped robot, a random target was marked on the floor. Similarly, a small bench was moved to random positions for the rover to reach. For both robots and in each trial, the user was instructed to point toward the target.

Table VI summarizes the success rate and mean errors over the 15 pointing trials for each robot. Errors were measured after the robot has stopped at the target and taken from the center of the marked target or bench to the center of the robot. The table also shows the mean distance of the robot from the desired target at the time of pointing. To test

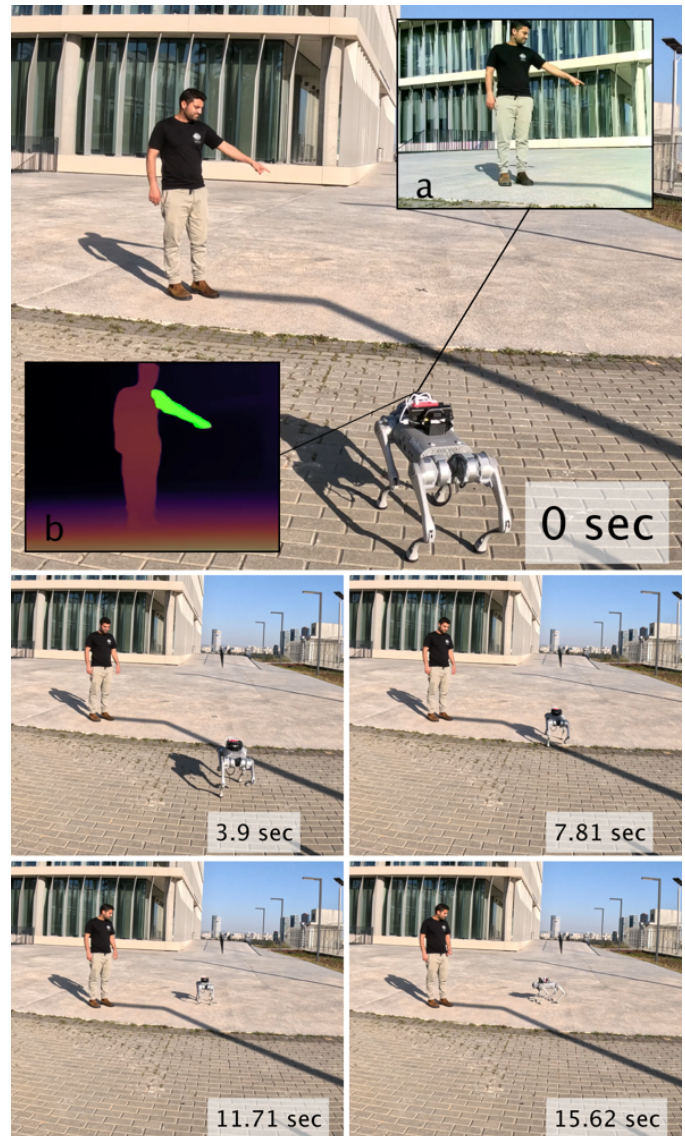


Fig. 24. Snapshots of a pointing experiment with the quadruped robot. The top image shows the moment of pointing along with (a) the image observed by the robot and (b) estimation of pointing direction. The robot reached the target with an accuracy of 0.09 m.

various scenarios, the tested distances for the rover were larger than for the quadruped robot. Figures 22-24 and Figure 25 show several pointing trials of the quadruped robot and rover, respectively. While the quadruped robot reached the vicinity of the target on all trials, the rover missed the bench two times. It is important to note that the reported deviations from the target are also a result of localization errors. The GPS-RTK of the quadruped robot suffered from localization drift and, therefore, errors are larger than for the rover over shorter travel distances. Similarly, some directive routes for the rover had lower mapping features for localization and, consequently, the rover missed two targets. Nevertheless, the results show that the pointing estimation provides sufficient accuracy for the robot to reach a user desired target through natural pointing and RGB images.

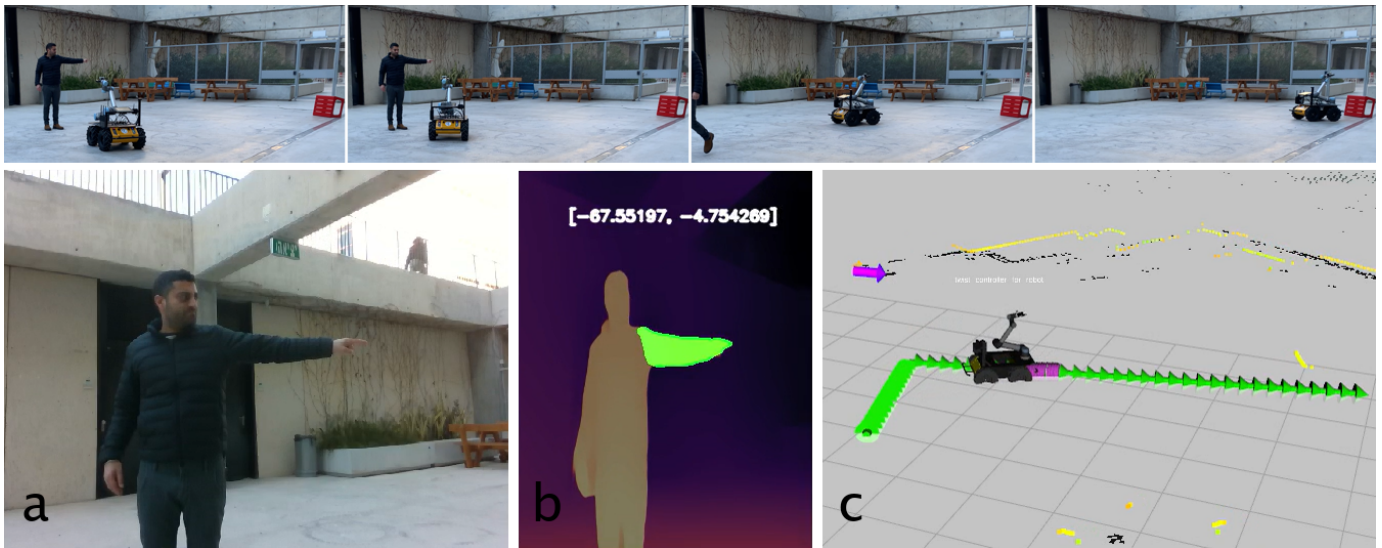


Fig. 25. Pointing experiment with a 4-wheel rover: (top row, left to right) the rover identifies pointing, plans motion and moves towards the target (red bench); (bottom row) (a) image observed by the rover, (b) estimation of pointing direction and (c) planning and controlling the motion in ROS-Gazebo. Purple arrow denotes the position and pointing direction estimation of the index finger with regards to the rovers map and at its initial pose. The rover reached the target with an accuracy of 0.3 m.

VII. CONCLUSIONS

In this work, a full framework was proposed for a robot to reason about a pointing user through an RGB camera and act to reach the pointed target. The framework includes the novel *PointingNet* model for recognition of a pointing gesture and estimation of its direction relative to the camera on the robot. The *PointingNet-S* model in the background segments any observed lifted arm in the image for further parsing by the two models. Arm segmentation by *PointingNet-S* along with MiDaS depth approximation have been shown to be crucial for accurate estimation of pointing position and direction. A comprehensive analysis over a large and diverse test set has validated the high accuracy of *PointingNet* compared to state-of-the-art approaches with skeleton-based models in particular. *PointingNet* was also successfully tested on possible edge cases such as occlusions and multiple participants in the observed image.

The experimental results over two robotic platforms have shown sufficient accuracy for the robot to reach a human desired target through natural pointing. In real-world scenarios, our natural pointing model can be accompanied with verbal instructions for the robot to reach a certain object or place. Verbal communication provides context regarding the desired task and can better direct the robot. We leave this for future efforts. Future work may also consider incorporating gaze estimation from the image during user glance at the target. As discussed in Section III, agile capturing will be required as users tend to take a very short glance at the desired target.

REFERENCES

- [1] K. Cooperrider, J. Slotta, and R. Núñez, "The preference for pointing with the hand is not universal," *Cognitive Science*, vol. 42, no. 4, pp. 1375–1390, 2018.
- [2] S. Kita, *Pointing: A foundational building block in human communication*. Mahwah, NJ: Lawrence Erlbaum, 2003.
- [3] M. Tomasello, *Origins of Human Communication*. The MIT Press, 08 2008.
- [4] E. Bates and F. Dick, "Language, gesture, and the developing brain," *Developmental Psychobiology*, vol. 40, no. 3, pp. 293–310, 2002.
- [5] G. Hewes, "Gesture language in culture contact," *Sign Language Studies*, vol. 4, no. 3, pp. 1–34, 1974.
- [6] H.-K. Lee and J.-H. Kim, "An hmm-based threshold model approach for gesture recognition," *IEEE Transactions on pattern analysis and machine intelligence*, vol. 21, no. 10, pp. 961–973, 1999.
- [7] N. H. Dardas and N. D. Georganas, "Real-time hand gesture detection and recognition using bag-of-features and support vector machine techniques," *IEEE Transactions on Instrumentation and measurement*, vol. 60, no. 11, pp. 3592–3607, 2011.
- [8] M. E. Hussein, M. Toriki, M. A. Gowayyed, and M. El-Saban, "Human action recognition using a temporal hierarchy of covariance descriptors on 3d joint locations," in *Twenty-third international joint conference on artificial intelligence*, 2013.
- [9] Y. Ji, Y. Yang, F. Shen, H. T. Shen, and X. Li, "A survey of human action analysis in hri applications," *IEEE Transactions on Circuits and Systems for Video Technology*, vol. 30, no. 7, pp. 2114–2128, 2020.
- [10] V. Villani, L. Sabatini, C. Secchi, and C. Fantuzzi, "A framework for affect-based natural human-robot interaction," in *IEEE International Symposium on Robot and Human Interactive Communication (RO-MAN)*, 2018, pp. 1038–1044.
- [11] D. Sikeridis and T. Antonakopoulos, "An imu-based wearable system for automatic pointing during presentations," *Image Processing & Communications*, vol. 21, 04 2017.
- [12] F. Haque, M. Nancel, and D. Vogel, "Myopoint: Pointing and clicking using forearm mounted electromyography and inertial motion sensors," in *Proceedings of the 33rd Annual ACM Conference on Human Factors in Computing Systems*, 2015, p. 3653–3656.
- [13] E. Littmann, A. Drees, and H. Ritter, "Neural recognition of human pointing gestures in real images," *Neural Process. Lett.*, vol. 3, no. 2, p. 61–71, 1996.
- [14] C.-B. Park and S.-W. Lee, "Real-time 3d pointing gesture recognition for mobile robots with cascade hmm and particle filter," *Image and Vision Computing*, vol. 29, no. 1, pp. 51–63, 2011.
- [15] K. Nagai, H. Sakabe, and M. Ohka, "Finger direction recognition toward human-and-robot cooperative tasks," in *International Symposium on Micro-NanoMechatronics and Human Science (MHS)*, 2017, pp. 1–3.
- [16] K. Nickel and R. Stiefelhagen, "Visual recognition of pointing gestures for human-robot interaction," *Image and Vision Computing*, vol. 25, no. 12, pp. 1875–1884, 2007.
- [17] D. Jirak, D. Biertimpel, M. Kerzel, and S. Wermter, "Solving visual object ambiguities when pointing: an unsupervised learning approach," *Neural Computing and Applications*, pp. 1–23, 2020.

- [18] A. Medeiros, P. Ratsamee, J. Orlosky, Y. Uranishi, M. Higashida, and H. Takemura, "3d pointing gestures as target selection tools: Guiding monocular uavs during window selection in an outdoor environment," *Robomech J*, vol. 8, no. 11, 2021.
- [19] C. Martin, F.-F. Steege, and H.-M. Gross, "Estimation of pointing poses for visually instructing mobile robots under real world conditions," *Robotics and Autonomous Systems*, vol. 58, no. 2, pp. 174–185, 2010.
- [20] D. Osokin, "Real-time 2d multi-person pose estimation on cpu: Lightweight openpose," 2018. [Online]. Available: <https://arxiv.org/abs/1811.12004>
- [21] C. Lugaresi, J. Tang, H. Nash, C. McClanahan, E. Uboweja, M. Hays, F. Zhang, C.-L. Chang, M. Yong, J. Lee, W.-T. Chang, W. Hua, M. Georg, and M. Grundmann, "Mediapipe: A framework for perceiving and processing reality," in *Third Workshop on Computer Vision for AR/VR at IEEE Computer Vision and Pattern Recognition (CVPR)*, 2019.
- [22] D. Mehta, S. Sridhar, O. Sotnychenko, H. Rhodin, M. Shafiei, H.-P. Seidel, W. Xu, D. Casas, and C. Theobalt, "VNect: Real-time 3d human pose estimation with a single RGB camera," *ACM Transactions on Graphics (TOG)*, vol. 36, no. 4, pp. 1–14, 2017.
- [23] Z. Cao, G. Hidalgo Martinez, T. Simon, S. Wei, and Y. A. Sheikh, "Openpose: Realtime multi-person 2d pose estimation using part affinity fields," *IEEE Transactions on Pattern Analysis and Machine Intelligence*, 2019.
- [24] C. Deuerlein, F. Müller, and P. Heß, "Case study of human pointing gestures and their data analysis," *Procedia CIRP*, vol. 88, pp. 223–228, 2020, 13th CIRP Conference on Intelligent Computation in Manufacturing Engineering, 17-19 July 2019, Gulf of Naples, Italy.
- [25] K. Hu, S. Canavan, and L. Yin, "Hand pointing estimation for human computer interaction based on two orthogonal-views," in *International Conference on Pattern Recognition*, 2010, pp. 3760–3763.
- [26] B. Azari, A. Lim, and R. T. Vaughan, "Commodifying pointing in hri: Simple and fast pointing gesture detection from rgb-d images," *Conference on Computer and Robot Vision (CRV)*, pp. 174–180, 2019.
- [27] Y. Lai, C. Wang, Y. Li, S. S. Ge, and D. Huang, "3d pointing gesture recognition for human-robot interaction," in *Chinese Control and Decision Conference (CCDC)*, 2016, pp. 4959–4964.
- [28] A. Kuramochi and T. Komuro, "3d hand pointing recognition over a wide area using two fisheye cameras," in *HCI International - Late Breaking Papers: Multimodality, eXtended Reality, and Artificial Intelligence*, 2021, pp. 58–67.
- [29] D. Shukla, O. Erkent, and J. Piater, "Probabilistic detection of pointing directions for human-robot interaction," in *International Conference on Digital Image Computing: Techniques and Applications (DICTA)*, 2015, pp. 1–8.
- [30] M. Tölgyessy, M. Dekan, F. Duchoň, J. Rodina, P. Hubinský, and L. Chovanec, "Foundations of visual linear human–robot interaction via pointing gesture navigation," *International Journal of Social Robotics*, vol. 9, pp. 509–523, 2017.
- [31] K. Pietroszek, L. Tahai, J. R. Wallace, and E. Lank, "Watchcasting: Freehand 3d interaction with off-the-shelf smartwatch," in *IEEE Symposium on 3D User Interfaces (3DUI)*, 2017, pp. 172–175.
- [32] S. S. Das, "Precise pointing direction estimation using depth data," in *IEEE International Symposium on Robot and Human Interactive Communication (RO-MAN)*, 2018, pp. 202–207.
- [33] R. Kehl and L. Van Gool, "Real-time pointing gesture recognition for an immersive environment," in *IEEE International Conference on Automatic Face and Gesture Recognition*, 2004, pp. 577–582.
- [34] J. Yang, W. Lu, and A. Waibel, "Skin-color modeling and adaptation," in *Computer Vision — ACCV'98*, R. Chin and T.-C. Pong, Eds., 1997, pp. 687–694.
- [35] L. Zhou, Z. Feng, Z. Cai, and X. Yang, "A Kinect-based finger pointing detection algorithm," in *Second IYSF Academic Symposium on Artificial Intelligence and Computer Engineering*, W. Qin, Ed., vol. 12079. International Society for Optics and Photonics, 2021, pp. 26 – 31.
- [36] J. Shotton, R. Girshick, A. Fitzgibbon, T. Sharp, M. Cook, M. Finocchio, R. Moore, P. Kohli, A. Criminisi, A. Kipman, and A. Blake, "Efficient human pose estimation from single depth images," *IEEE Transactions on Pattern Analysis and Machine Intelligence*, vol. 35, no. 12, pp. 2821–2840, 2013.
- [37] Z. Khokhar, Z. Xiao, and C. Menon, "Surface EMG pattern recognition for real-time control of a wrist exoskeleton," *Biomedical engineering online*, vol. 9, p. 41, Aug. 2010.
- [38] J. DelPreto and D. Rus, "Plug-and-play gesture control using muscle and motion sensors," in *ACM/IEEE International Conference on Human-Robot Interaction*, 03 2020, pp. 439–448.
- [39] N. Caruana, C. Inkley, P. Nalepka, D. Kaplan, and M. Richardson, "Gaze facilitates responsibility during hand coordinated joint attention," *Scientific Reports*, vol. 11, no. 1, pp. 1–11, 2021.
- [40] A. G. Goma, G. Reyes, A. Alles, L. H. Rupp, and M. Feld, "Studying person-specific pointing and gaze behavior for multimodal referencing of outside objects from a moving vehicle," *Proceedings of the 2020 International Conference on Multimodal Interaction*, pp. 501–509, 2020.
- [41] J. Gonzalez-Billandon, G. Belgiovine, M. Tata, A. Sciutti, G. Sandini, and F. Rea, "Self-supervised learning framework for speaker localisation with a humanoid robot," in *IEEE International Conference on Development and Learning (ICDL)*, 2021, pp. 1–7.
- [42] J. Han, P. Fang, W. Li, J. Hong, M. A. Armin, I. Reid, L. Petersson, and H. Li, "You only cut once: Boosting data augmentation with a single cut," in *International Conference on Machine Learning (ICML)*, 2022.
- [43] S. Zagoruyko and N. Komodakis, "Wide residual networks," *arXiv preprint arXiv:1605.07146*, 2016.
- [44] A. Krizhevsky, I. Sutskever, and G. E. Hinton, "Imagenet classification with deep convolutional neural networks," *Communications of the ACM*, vol. 60, no. 6, pp. 84–90, 2017.
- [45] C. Szegedy, W. Liu, Y. Jia, P. Sermanet, S. Reed, D. Anguelov, D. Erhan, V. Vanhoucke, and A. Rabinovich, "Going deeper with convolutions," in *Proceedings of the IEEE conference on computer vision and pattern recognition*, 2015, pp. 1–9.
- [46] V. Bazarevsky, I. Grishchenko, K. Raveendran, T. Zhu, F. Zhang, and M. Grundmann, "Blazepose: On-device real-time body pose tracking," *arXiv preprint arXiv:2006.10204*, 2020.
- [47] R. Ranftl, K. Lasinger, D. Hafner, K. Schindler, and V. Koltun, "Towards robust monocular depth estimation: Mixing datasets for zero-shot cross-dataset transfer," *IEEE Transactions on Pattern Analysis and Machine Intelligence (TPAMI)*, 2020.
- [48] R. Ranftl, A. Bochkovskiy, and V. Koltun, "Vision transformers for dense prediction," *ArXiv preprint*, 2021.
- [49] Z. Liu, H. Mao, C.-Y. Wu, C. Feichtenhofer, T. Darrell, and S. Xie, "A convnet for the 2020s," in *Proceedings of the IEEE/CVF Conference on Computer Vision and Pattern Recognition*, 2022, pp. 11 976–11 986.
- [50] S. M. LaValle, *Planning Algorithms*. Cambridge University Press, 2006.
- [51] S. Karimipouli and P. Tahmasebi, "Segmentation of digital rock images using deep convolutional autoencoder networks," *Computers & Geosciences*, vol. 126, pp. 142–150, 2019.
- [52] O. Ronneberger, P. Fischer, and T. Brox, "U-net: Convolutional networks for biomedical image segmentation," in *Medical Image Computing and Computer-Assisted Intervention—MICCAI 2015: 18th International Conference, Munich, Germany, October 5-9, 2015, Proceedings, Part III 18*. Springer, 2015, pp. 234–241.
- [53] Z. Zhou, M. M. R. Siddiquee, N. Tajbakhsh, and J. Liang, "Unet++: Redesigning skip connections to exploit multiscale features in image segmentation," *IEEE transactions on medical imaging*, vol. 39, no. 6, pp. 1856–1867, 2019.
- [54] T.-Y. Lin, P. Dollár, R. Girshick, K. He, B. Hariharan, and S. Belongie, "Feature pyramid networks for object detection," in *Proceedings of the IEEE conference on computer vision and pattern recognition*, 2017, pp. 2117–2125.
- [55] K. He, X. Zhang, S. Ren, and J. Sun, "Deep residual learning for image recognition," in *Proceedings of the IEEE conference on computer vision and pattern recognition*, 2016, pp. 770–778.
- [56] G. Huang, Z. Liu, L. Van Der Maaten, and K. Q. Weinberger, "Densely connected convolutional networks," in *Proceedings of the IEEE conference on computer vision and pattern recognition*, 2017, pp. 4700–4708.
- [57] L.-C. Chen, Y. Zhu, G. Papandreou, F. Schroff, and H. Adam, "Encoder-decoder with atrous separable convolution for semantic image segmentation," in *Proceedings of the European conference on computer vision (ECCV)*, 2018, pp. 801–818.
- [58] K. Simonyan and A. Zisserman, "Very deep convolutional networks for large-scale image recognition," *arXiv preprint arXiv:1409.1556*, 2014.